International Journal of Nanomedicine

Dovepress
open access to scientific and medical research

Open Access Full Text Article

ORIGINAL RESEARCH

Encapsulating Halofuginone Hydrobromide in TPGS Polymeric Micelles Enhances Efficacy Against Triple-Negative Breast Cancer Cells

This article was published in the following Dove Press journal:
International Journal of Nanomedicine

Runan Zuo[1]
Jingjing Zhang[1]
Xinhao Song[1]
Shiheng Hu[1]
Xiuge Gao[1]
Junqi Wang[1]
Hui Ji[1]
Chunlei Ji[1]
Lin Peng[1]
Hongbin Si[2]
Gonghe Li[2]
Kun Fang[3]
Junren Zhang[1]
Shanxiang Jiang[1]
Dawei Guo[1]

[1]Center for Veterinary Drug Research and Evaluation, MOE Joint International Research Laboratory of Animal Health and Food Safety, College of Veterinary Medicine, Nanjing Agricultural University, Nanjing, 210095, People's Republic of China; [2]College of Animal Science and Technology, Guangxi University, Nanning, 530004, People's Republic of China; [3]Division of Life Sciences and Medicine, The First Affiliated Hospital of USTC, University of Science and Technology of China, Hefei, 230001, People's Republic of China

Correspondence: Dawei Guo; Shanxiang Jiang
Center for Veterinary Drug Research and Evaluation, MOE Joint International Research Laboratory of Animal Health and Food Safety, College of Veterinary Medicine, Nanjing Agricultural University, 1 Weigang, Nanjing, 210095, People's Republic of China
Tel + 86-25-84396215
Fax + 86-25-84398669
Email gdawei0123@njau.edu.cn; nauvy@sina.com

Background: Halofuginone hydrobromide (HF) is a synthetic analogue of the naturally occurring quinazolinone alkaloid febrifugine, which has potential therapeutic effects against breast cancer, however, its poor water solubility greatly limits its pharmaceutical application. D-α-tocopherol polyethylene glycol 1000 succinate (TPGS) is a water-soluble derivative of vitamin E, which can self-assemble to form polymeric micelles (PMs) for encapsulating insoluble anti-tumor drugs, thereby effectively enhancing their anti-cancer effects.

Methods: HF-loaded TPGS PMs (HTPMs) were manufactured using a thin-film hydration technique, followed by a series of characterizations, including the hydrodynamic diameter (HD), zeta potential (ZP), stability, drug loading (DL), encapsulation efficiency (EE), and in vitro drug release. The anti-cancer effects and potential mechanism of HTPMs were investigated in the breast cell lines MDA-MB-231 and MCF-7, and normal breast epithelial cell line Eph-ev. The breast cancer-bearing BALB/c nude mouse model was successfully established by subcutaneous injection of MDA-MB-231 cells and used to evaluate the in vivo therapeutic effect and safety of the HTPMs.

Results: The optimized HTPMs had an HD of 17.8±0.5 nm and ZP of 14.40±0.1 mV. These PMs exhibited DL of 12.94 ± 0.46% and EE of 90.6 ± 0.85%, along with excellent storage stability, dilution tolerance and sustained drug release in pH-dependent manner within 24 h compared to free HF. Additionally, the HTPMs had stronger inhibitory effects than free HF and paclitaxel against MDA-MB-231 triple-negative breast cancer cells, and little toxicity in normal breast epithelial Eph-ev cells. The HTPMs induced cell cycle arrest and apoptosis of MDA-MB-231 by disrupting the mitochondrial membrane potential and enhancing reactive oxygen species formation. Evaluation of in vivo anti-tumor efficacy demonstrated that HTPMs exerted a stronger tumor inhibition rate (68.17%) than free HF, and exhibited excellent biocompatibility.

Conclusion: The findings from this study indicate that HTPMs holds great clinical potential for treating triple-negative breast cancer.

Keywords: halofuginone hydrobromide, triple-negative breast cancer, TPGS, polymer micelles

Introduction

Breast cancer is the most deadly cancer among women, causing significant morbidity and mortality worldwide.[1] Currently, this disease is the most common cancer in Chinese women.[1,2] As with the case of all solid tumors, breast cancer is a complex disease that is difficult to treat. Breast cancer is usually classified by the presence, or absence of three receptors: estrogen receptor, progesterone

receptor, and human epidermal growth factor receptor 2.[3–5] These three receptors are the most frequently used biomarkers for breast cancer targeted drug delivery. The therapeutic approach for breast cancer is highly influenced by the ability of therapeutic agents to specifically target these receptors. Triple-negative breast cancer (TNBC) that lacks all three receptors is one of the most difficult breast cancers to treat. In particular, TNBC is a heterogeneous disease characterized by aggressive biology and poor prognosis.[6] The lack of tumor-specific markers, aggressive nature, and special propensity to recur and metastasize, making TNBC more difficult to treat compared to other subtypes. Currently, radiation therapy, surgery, chemotherapy and combined chemotherapeutic regimens are the most successful treatments available, leading to higher survival rates compared to other treatments.[7] However, although there are a wide variety of anti-cancer drugs, such as chemical drugs, they often have low efficacy and high toxicity, and can cause strong drug resistance in patients.[8] The most widely prescribed chemotherapeutic agent for breast cancer is paclitaxel (PTX), also known as Taxol.[9] PTX acts by enhancing tubulin polymerization, which further hyperstabilizes microtubules, leading to interference with cell proliferation and programmed cell death.[10] Although widely used to treat breast cancer, PTX is nonselective and has rapid systemic clearance and multidrug resistance, limiting its clinical efficacy.[11]

Halofuginone hydrobromide (HF) is a small molecule alkaloid derived from febrifugine.[12,13] The therapeutic functions of HF range from anti-inflammatory to anti-fibrosis and even anti-cancer.[14,15] HF suppresses cancer cell growth and decreases tumor metastasis in hepatoma, melanoma, and multiple myeloma in vitro.[16] In one preclinical trial, HF was used as an anti-carcinogenic drug for advanced solid tumors.[17] Subsequent research in vivo also has demonstrated the function of HF in suppressing growth and angiogenesis of gliomas in rats, growth of hepatocellular carcinoma in mice, and osteosarcoma growth and lung metastases in a preclinical BALB/c nude model.[16,18] However, HF has poor solubility in water, which affects its bioavailability and clinical efficacy. Therefore, it is urgent to solve this issue to enhance the clinical therapeutic potential. A recent study showed that HF is the substrate of two efflux proteins, ATP-binding cassette super-family G member 2 (Abcg2) and Abcb1, possibly influencing its cellular uptake in intestinal epithelial cells and breast cancer cells.[19]

Compared with other drug delivery systems, nanocarriers have multiple advantages, such as targeting, long-action time, low toxic effect, and wide drug-loading (DL) capacity.[20,21] Polymer micelles (PMs) can be self-assembled to form nanoparticles with a hydrophobic core and a hydrophilic shell. As a new type of drug vehicle, PMs have a high DL capacity, stable structure, long retention time in the body, and few adverse effects. D-α-tocopherol polyethylene glycol 1000 succinate, referred to as TPGS, is an excellent emulsifier, stabilizer, and penetration enhancer, and also protects micelles.[22] TPGS not only increases drug stability, drug penetration and absorption, but also improves therapeutic effects.[5,23,24] Importantly, TPGS can self-assemble to form PMs with anti-dilution effects compared with surfactant micelles. Anti-tumor drugs are not only enriched passively in cancer tissues due to the enhanced permeability and retention effect (EPR) but can also be used to achieve targeted drug delivery by modifying the surface groups of the PMs. Simultaneously, TPGS can reverse multidrug resistance (MDR) by blocking the efflux of P-glycoprotein (P-gp), thereby enhancing the treatment effect of anti-tumor drugs. As HF is a substrate of P-gp, TPGS PMs can possibly contribute to its intracellular enrichment.

In this study, we developed the TPGS based PMs to deliver HF to enhance the therapeutic effects on TNBC. The thin film ultrasonic technique was first used to screen the optimized preparation of HF-loaded TPGS PMs (HTPMs) according to the hydrodynamic diameter (HD), polydispersity index (PDI) and zeta potential (ZP). The optimized HTPMs were further characterized for surface morphology, encapsulation efficiency (EE), DL and in vitro drug release profile. Subsequently, the in vitro anti-cancer effect of HTPM was compared to that of HF and PTX against the MDA-MB-231 and MCF-7 cell lines. The potential anti-tumor mechanism of HTPMs was investigated in terms of cell apoptosis, cell cycle arrest, reactive oxygen species (ROS) and mitochondrial membrane potential (MMP). The in vivo anti-tumor efficacy and safety of HTPMs were ultimately confirmed using subcutaneous tumor-bearing mouse models after intravenous (IV.) administration.

Materials and Methods

Materials

HF was purchased from Shanxi Meixilin Pharmaceutical Co., Ltd. (Yuncheng, China). TPGS was purchased from Guangzhou Kafen Biological Technology Co., Ltd.,

(Guangzhou, China). PTX was purchased from Dalian Meilun Biological Technology Co., Ltd. (Dalian, China). Fetal bovine serum (FBS) and an MMP detection kit were provided from Nanjing Shanben Biotechnology Co., Ltd., (Nanjing, China). Dulbecco's Modified Eagle's Medium (DMEM), penicillin, trypsin, and streptomycin were obtained from Hyclone Laboratories (Logan, UT, USA). An apoptosis detection kit, cell cycle detection kit and ROS detection kit were purchased from Nanjing Kaiji Biotechnology Co., Ltd (Nanjing, China). All other reagents and chemicals were of analytical grade.

Cell Line Culture

Breast cancer cell lines MDA-MB-231 and MCF-7 and the normal mouse mammary epithelial line Eph-ev were maintained in DMEM supplemented with 1% penicillin, 1% streptomycin and 10% FBS. All cells were purchased from the Type Culture Collection of the Chinese Academy of Sciences (Shanghai, China). All cells were cultured in an cell incubator with 5% CO_2 at 37°C.

Preparation of HTPMs

HF-loaded TPGS polymer micelles (HTPMs) were prepared by the thin film ultrasonic method. Methanol was first screened out as an excellent solvent of both HF and TPGS. Subsequently, various rates of HF and TPGS were added to methanol to acquire the transparent organic phase. Then the organic phase was gradually evaporated, and a thin film was formed on the surface of the distillation flask. The de-ionized water was further added to the distillation flask, followed by probe ultrasonic (300 mV, 20 min) to acquire the PMs.

Analysis of HD, ZP, and PDI

The HD, ZP, and PDI of HTPM were determined by dynamic light scattering (DLS) with a Zetasizer (Nano ZS90; Malvern Instruments Ltd., Malvern, UK). The samples at suitable concentrations were measured with scattering angles of 90° at 25°C.

Transmission Electron Microscopy

The morphology of the HTPMs was determined by transmission electron microscopy (TEM, JEM-1200EX; JEOL Ltd., Tokyo, Japan). One drop of PM solution was fixed on a copper grid, dried at room temperature and observed by TEM.

DL and EE

The HTPM was filtered through a micropore filter (0.22 μm) to collect the filtrate, and 1 mL was taken for ultraviolet (UV) spectrophotometry (UV-1900; Shimadzu Instruments (Suzhou) Co., Ltd., Beijing, China) to determine the concentrations of HF in the filtrate. The DL and EE of the PMs were calculated according to the following formula.

$$DL(\%)=WE/WT \times 100\%$$

$$EE(\%)= WE/WD \times 100\%,$$

where WE, WT, and WD represent the amounts of encapsulated drugs, total drug amounts, and total amounts of PMs.

Stability Evaluation

The as-prepared HTPM solution was maintained at 40°C with a relative humidity of 75%. The samples were collected on days 0, 7, 14, 21, 28, 35, 42, 49, and 56 and their HDs, ZPs, and PDI were measured to evaluate the storage stability of HTPM. The prepared HTPM was diluted by 0-, 50-, 100-, 200-, 500-, 800-, and 1000-fold, to investigate their dilution effects by determining their HDs, ZPs, and PDI.

In vitro Release of HTPMs

The in vitro release behavior of PMs was studied by the dialysis bag method. Drug loaded micelle solution (5mL) was precisely measured and placed in a dialysis bag. Then the drug-loaded micelle solution went incubated at temperature oscillation at 37 ± 0.5°C and 100 rpm. The release medium (1 mL) was taken at 30 min, 1, 2, 3, 4, 6, 8, 10, 12 and 24 h and added to fresh release medium (1 mL). The concentrations of HF in the release medium were determined by UV spectrophotometry (UV-1900; Shimadzu Instruments (Suzhou) Co., Ltd.). Finally, the release percentage was calculated to investigate the release characteristics of drug-loaded micelles.

Cell Viability

Cell viability was determined using the Cell Counting Kit-8 (CCK-8) method. Eph-ev, MDA-MB-231, and MCF-7 cells were adjusted to densities of 1×10^5 cells/mL, 1×10^5 cells/mL, and 2×10^5 cells/mL, respectively, and seeded in a 96-well plate in 100 μL medium with five replicates. These 96-well plates were placed overnight in 5% CO_2 incubator at 37°C. PTX, HF and HTPM were added, and incubated for 24, 48, and 72 h. Then, 10 μL CCK-8 solution was added to each well and incubated at 37°C

for 4 h, and the absorbance of each well at 450 nm was measured. Cell viability was calculated according to the following formula: cell viability (%) = ($OD_{treated}$ − OD_{blank})/($OD_{untreated}$ − OD_{blank}) × 100%.

Cell Apoptosis

Cells were seeded in a 12-well plate and cultured overnight. After pre-treatment with N-acetyl-L-cysteine (NAC) for 1 h, the cells were co-incubated with HTPMs at various concentrations for 24 h. The cells were collected, washed twice with ice-cold phosphate buffered saline (PBS), and resuspended in 500 μL binding buffer. Annexin V-FITC and propidium iodide (PI) solution (5 μL, 200 μg/mL) were incubated with the cell suspension in the dark for 15 min at 37°C, and cells were analyzed using a cell cytometer (BD Biosciences, New York, USA). Cell-Quest software (Becton Dickinson San Jose, CA, USA) was employed to analyze the data.

Cell Cycle

MDA-MB-231 cells and MCF-7 cells were seeded at a density of 1×10^5 cells/well in 12-well plates and incubated overnight. Subsequently, after pre-treatment with NAC for 1 h, the cells were co-incubated with HTPM at various concentrations for 24 h. Upon completion of the treatment, the cells were harvested by trypsinization, fixed in 70% ethanol and incubated overnight at 4°C. Next, the cells were treated with RNase A, stained with PI and analyzed using a FACS Calibur (BD Biosciences).

Reactive Oxygen Species

ROS levels were evaluated using an ROS assay kit based on 2′,7′-Dichlorodihydrofluorescin diacetate (DCFH-DA). MDA-MB-231 and MCF-7 cells were treated with H_2O_2 (100 μM) and HTPM (0, 0.78, 3.13, 12.5 and 50 nM) for 12 h after pre-treatment with NAC for 1 h, and then incubated with DCFH-DA (50 μM) for 50 min in the dark. The fluorescence was finally analyzed with a flow cytometer (BD Biosciences).

Mitochondrial Membrane Potentials

JC-1 (5, 5, 6, 6-tetrachloro-1, 1, 3, 3-tetraethylbenzimidazolylcarbo-cyanine iodide) dye (Molecular Probes, Eugene, OR, USA) was used to assess changes in the MMPs. MDA-MB-231 and MCF-7 cells (1×10^5 cells/well) were cultured in 12-well plates and then treated with HTPM at various concentrations for 24 h after pre-treatment with NAC for 1 h. Subsequently, the cells were collected and washed with PBS. JC-1 reagent (10 μg/mL) was added to each sample and incubated at 37°C in the dark for 15 min. The fluorescence was finally analyzed with a flow cytometer (BD Biosciences, FACS Aria, Heidelberg, Germany).

Animal Tumor Xenograft Model

BALB/c nude mice (4 weeks old, female) were obtained from the Laboratory Animal Center of Yangzhou University (Yangzhou, China), and fed in the Laboratory Animal Center of Nanjing Agricultural University (Nanjing, China). Animal experiments were conducted according to the Guidelines for Animal Experimentation of Nanjing Agricultural University, and the protocol was approved by the Animal Ethics Committee of this institution (No. 2020014). To establish the MDA-MB-231 xenograft models, MDA-MB-231 cells (1×10^6 cells/mouse) were subcutaneously injected into the flanks of the nude mice.

In vivo Anti-Tumor Effect

The anti-breast cancer activity of HTPM was investigated using MDA-MB-231 tumor-bearing mice. When the tumor volumes reached 50–100 mm^3, MDA-MB-231 tumor-bearing mice were weighed and assigned randomly to the following groups: HF, HTPM, and control (PBS). Then the nude mice were injected via the tail vein with equivalent doses of 0.25 mg/kg HF or HTPM on days 0, 2, 4, 6, 8, and 10. The body weight and tumor size for each mouse were measured every 2 days until day 14. At the end of the experiment, the mice were sacrificed to obtain the tumor samples. Hematoxylin and eosin (H&E) was used to stain the main organs and tumor tissues for pathological analysis. TUNEL staining was utilized to detect the apoptosis of tumor tissues. The tumor inhibition rate (TIR) was calculated according to the following formula:

TIR = (1−VD/VB) ×100%,

where VD and VB represent the mean tumor size in the dosed group and vehicle group, respectively.

Statistical Analysis

GraphPad Prism 6.0 (La Jolla, CA, USA) was used to analyze the data. The Student's *t*-test was used to analyze the data between two groups. The data are shown as the mean ± standard deviation. $P < 0.05$ was considered statistically significant.

Results and Discussion

HF Exhibits Strong Inhibitory Effects Against Breast Cancer Cells

HF has significant therapeutic potential against multiple malignant tumors.[25,26] In this study, the cytotoxic effects of HF on breast cancer cells were evaluated by the CCK-8 assay. As shown in Figure 1A–C, the viability of MDA-MB-231 cells was gradually decreased with increasing treatment times and concentrations of HF. Similar results occurred in MCF-7 cells. These data demonstrate that HF can inhibit the growth of breast cancer cells including TNBC cells in time- and concentration-dependent manners.[25] We further found that HF exhibited a stronger anti-proliferative activity than the traditional tumor therapeutic drug PTX against MDA-MB-231 and MCF-7 cells (Figure 1A–F). More importantly, HF had less inhibitory effects on non-tumorigenic breast epithelial cells Eph-ev than breast cancer cell lines (Figure 1G–I), supporting the selective cytotoxic effects of HF on breast cancer cells. In addition, HF inhibited the migration and invasion of breast cancer cells through the downregulation of matrix metalloproteinase-9 expression and its upstream transcription factors.[25] Therefore, HF is a promising agent for breast cancer chemotherapy.

Characterization of HTPMs

The amphiphilic nature of TPGS drives its self-assembly into PMs in aqueous buffer to encapsulate poorly water-soluble drugs.[22] In this study, HTPMs were prepared using the thin-film ultrasonic process (Supplemental Materials, Figure S1). The particle sizes and surface features of the PMs are of importance for drug release, cellular uptake, and accumulation in tumor tissues.[27] Thus, the HD, PDI, and ZP were determined by DLS, and these parameters of HTPM varied with different rates of HF and TPGS (Figure 2A). When the weight ratio was 6, the optimal formulation of HTPM had the smallest HD (Figure 2B) and the highest ZP (Figure 2C), which were 17.8 ± 0.5 nm and 14.40 ± 0.1 mV, respectively. Small-sized PMs < 200 nm are more suitable for the accumulation of anti-tumor drugs inside tumor tissues due to the EPR effect.[28] The surface charges of micelles are also critical to the transport of drugs across tumor cell

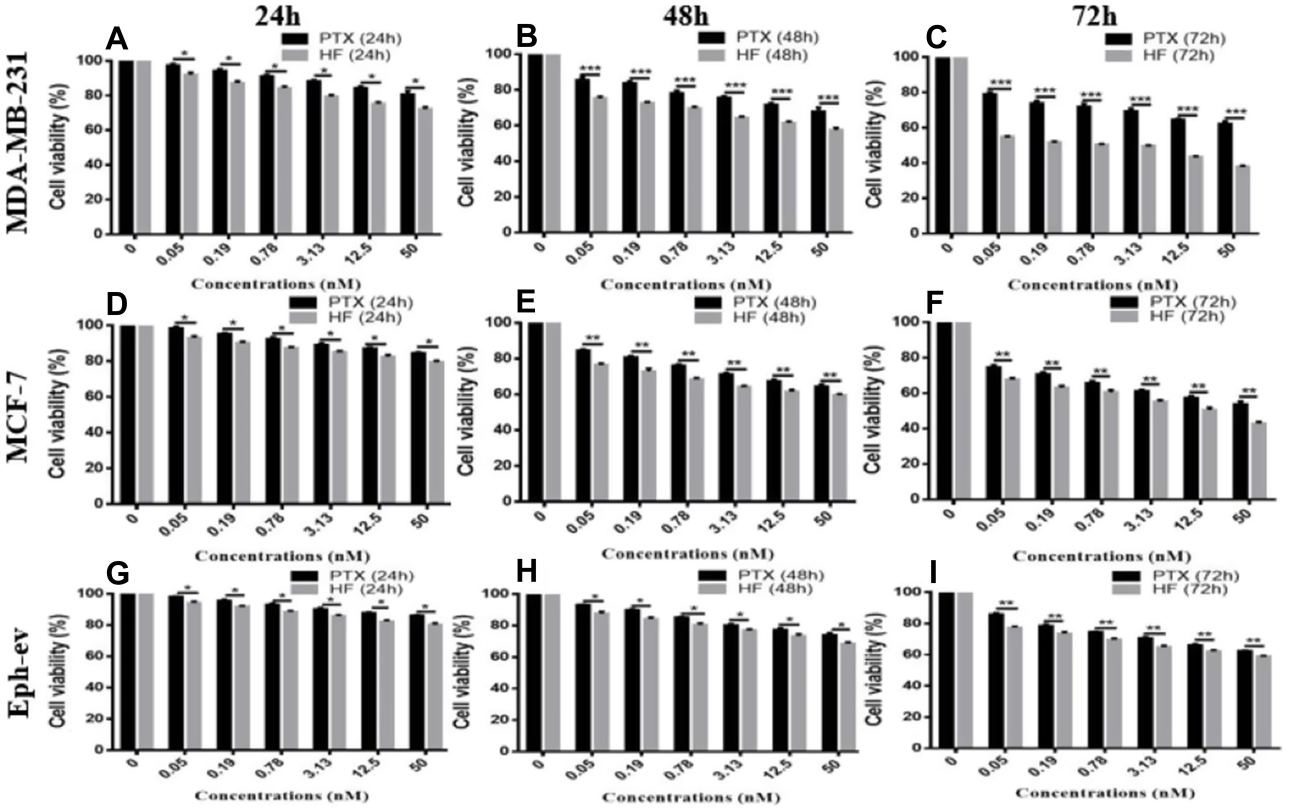

Figure 1 Effect of HF or PTX on the viability of MDA-MB-231 cells, MCF-7 cells and Eph-ev cells. MDA-MB-231 cells (**A**–**C**), MCF-7 cells (**D**–**F**) and Eph-ev cells (**G**–**I**) were dealt with different concentration (from 0 to 50 nM) of HF or PTX in 24 h, 48 h and 72 h. **P*<0.05, ***P*<0.01, ****P*<0.001.

membranes. In particular, the positive charge of micelles results in the enhanced interplay with negative charge and intracellular uptake.[3] High ZP contributed to stabilizing the HTPM in solution, which was further demonstrated by the PDI of 0.212 ± 0.1. A PDI < 0.3 is generally considered a narrow size distribution, while a PDI > 0.3 indicates a broad size distribution.[29] TEM was utilized to further evaluate the morphology and size of the HTPMs, which appeared spherical with homogeneous distribution (Figure 2D), further indicating the excellent stability of HTPM.

The DL% and EE% are key parameters of PMs influencing drug accumulation at tumor sites.[30] In this study, HTPM had DL of 90.6 ± 0.85% and EE of 12.94 ± 0.46% (Figure 3A), indicating that TPGS PMs are exceptional delivery carriers of HF. The sustained and controlled release is of importance to enhance the drug bioavailability for tumor therapy. Therefore, the release profiles of HTPM in PBS with various pH values were determined by the dialysis bag method (Figure 3B). The results showed that the cumulative release percentage (CRP) of HF from HTPM was approximately 70.5% within 24 h at pH 7.4, whereas that of free HF was 92.5%, suggesting that HTPM had an excellent sustained release effect conducive to the accumulation of drugs in the tumor microenvironment. The pH in the breast cancer microenvironment is usually about 6.5.[31] Under this pH environment, the CRP of HF from HTPMs increased to approximately 80.48% within 24 h, indicating that weakly acidic environments improve the HF release rate from HTPM, which beneficial for treating acidic cancer cells.[32] In addition, there was no burst release from the HTPMs, further demonstrating that TPGS PMs have a high EE for HF. The pharmacokinetic properties of free HF are reflected in the low blood concentration and fast distribution. Relevant literature has separately reported the pharmacokinetic studies of free HF by oral, intraperitoneal, and intravenous injection.[33]

The stability of HTPM was subsequently evaluated based on variation in the HD, ZP, and PD. As shown in Figure 3C, these parameters varied less than 5% at 40°C during the 56-day storage period, indicating that it can be stored stably for a long time. Meanwhile, the dilution stability of HTPM was assessed when the original solution was diluted by 0-, 50-, 100-, 200-, 500-, 800-, and 1000-fold. The results showed that their HD, ZP, and PDI

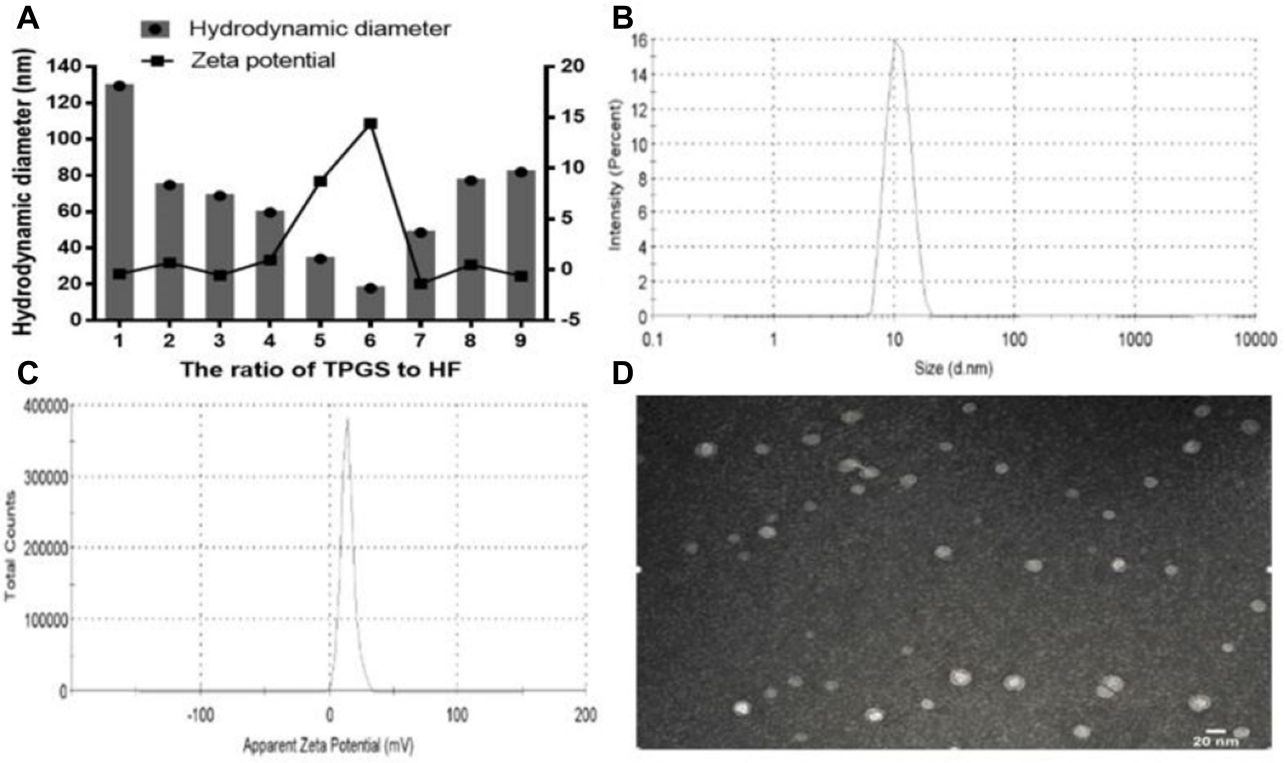

Figure 2 Screening and characterization of the optimal HTPM. (**A**) The optimal formulation of HTPM was screened by altering the ratio of TPGS and HF. (**B** and **C**) Hydrodynamic diameters and zeta potentials of HTPM were determined by dynamic light scattering. (**D**) The surface morphology of HTPM was observed by transmission electron microscopy, which appeared spherical.

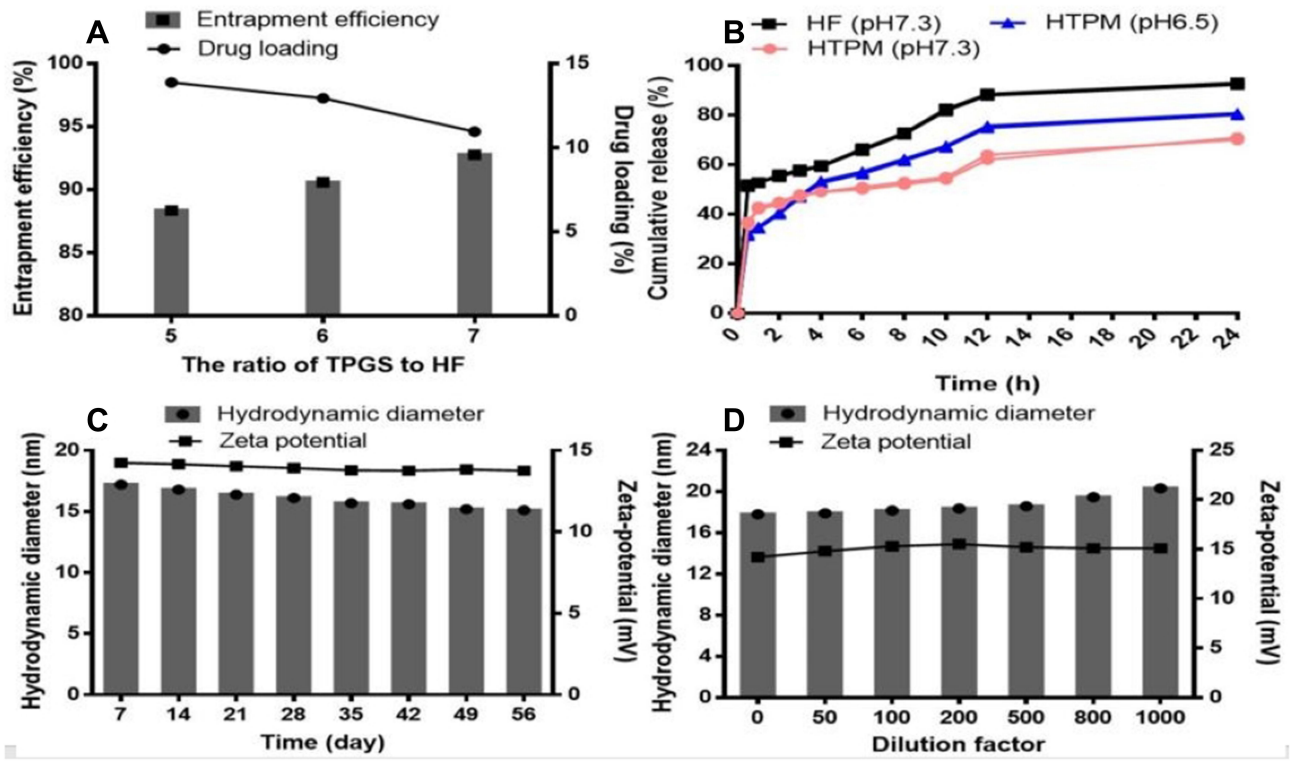

Figure 3 Drug loading, entrapment efficiency (**A**), in vitro release (**B**), storage stability (**C**) and dilution tolerance (**D**) of the optimal HTPM.

did not significantly change under various dilution conditions (Figure 3D), revealing it has excellent anti-dilution effects.

In vitro Anti-Proliferative Effects

HTPM Has Inhibitory Effects Against Breast Cancer Cells

The viability of breast cancer cells and non-tumorigenic breast epithelial cells treated with HTPM for various times were further investigated using the CCK-8 assay. The results showed that HTPM decreased the viability of MDA-MB-231 cells (Figure 4A), MCF-7 cells (Figure 4B) and Eph-ev cells (Figure 4C) in time- and concentration-dependent manners similar to HF. HTPM exhibited stronger inhibitory effects against all three cell lines compared with free HF (Figure 1). Small-sized particles can enhance the intracellular delivery of therapeutic drugs. In addition, TPGS has evident effects on the inhibition of verapamil-induced P-gp ATPase activity,[34] and HF is a substrate of P-gp.[19] Therefore, TPGS PMs can result in higher cellular uptake and more significant cytotoxic effects than the free HF solution.

Apoptosis Induced by HTPMs

Apoptosis is involved in the cytotoxic mechanism of HF on breast cancer cells.[25] To further determine how HTPM reduces the viability of breast cancer cells, Annexin V-FITC/PI double staining was performed to assess the extent and mode of cell death.[35] In this study, MDA-MB-231 cells were treated with various concentrations of HPTM ranging from 0 to 50 nM, and then the percentage of apoptotic cells was quantitatively analyzed by flow cytometry. As depicted in Figure 5A–B, HTPM lead to apoptosis, including early and late apoptosis after exposure for 24 h. The apoptotic levels of MDA-MB-231 cells were gradually enhanced with increased treatment concentrations. When the exposed concentration of HTPM was 50 nM, the percentage of apoptotic cells was up to 48%. These results were verified in MCF-7 cells (Supplementary Materials, Figure S3A and B). Although HTPM can also lead to the apoptosis of Eph-ev cells in a dose-dependent manner, the proportion of apoptotic cells was significantly lower than that of cancer cells exposed to the same concentration of HTPM. For example, the apoptotic level of Eph-ev cells was only 12.1% after treatment with 50 nM HTPM (Supplementary Materials, Figure S2),

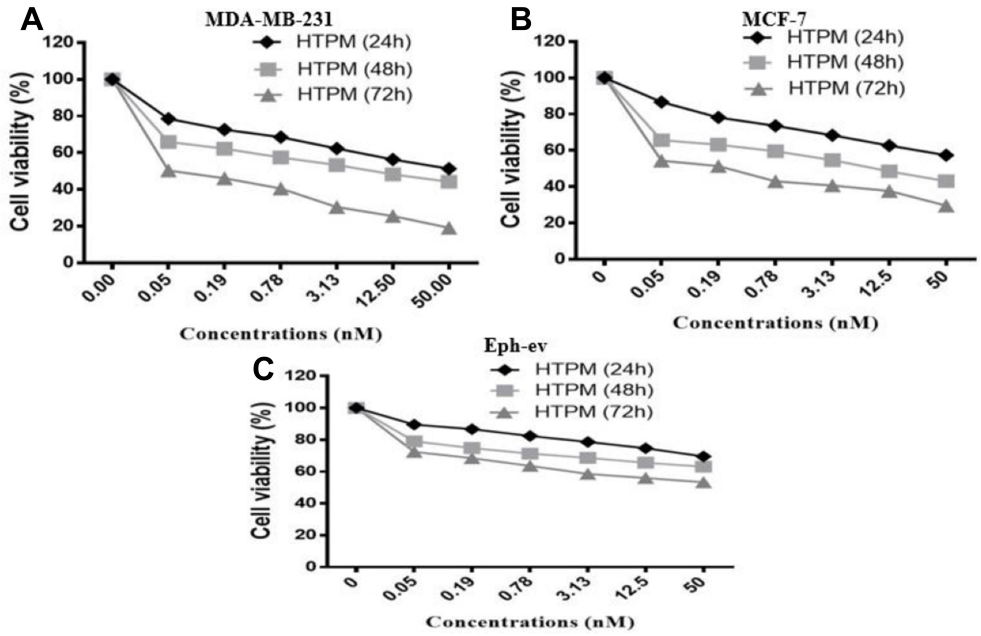

Figure 4 Inhibition of HTPM on the growth of MDA-MB-231 cells, MCF-7 cells and Eph-ev cells. MDA-MB-231 cells (**A**), MCF-7 cells (**B**) and Eph-ev cells (**C**) were treated with various concentrations (from 0 to 50nM) of HTPM in 24 h, 48 h and 72 h.

in line with the results of the viability of Eph-ev cells influenced by HTPM.

Cell Cycle Altered by HTPM Exposure

The cell cycle is intimately related to apoptosis, and the parameters related to the cell cycle are evaluated to better understand the preliminary mechanism of drug-induced apoptosis. The cell cycle is the basis of cell life activity and controls the entry of the stationary phase into the proliferative phase.[36] HF destroys microtubules, resulting in the significant arrest of cancer cells in the G2-M phase and subsequent apoptosis.[17] Herein, cell cycle analysis was carried out by determining the DNA content of the untreated and treated cells by flow cytometry. The results showed that the DNA content of the G2-M phase was enhanced, whereas that of the G0-G1 phase was decreased in MDA-MB-231 cells upon exposure to HTPM for 24 h (Figure 5C). Specifically, the DNA contents of the G2-M phase were 18.26% for 12.5 nM and 20.45% for 50 nM HTPM treatment (Figure 5C) compared with the control group (1.41%). Similar results were found in MCF-7 cells (Supplementary Materials, Figure S3C). The DNA content of the S phase was increased to 58.22% after treatment with NAC, further showing that the cells were arrested in the G2-M phase and proliferated in the S phase (bloom phase of DNA replication). These findings were also observed in MCF-7 cells (Supplementary Materials, Figure S3C).

Generation of ROS by HTPM Exposure

ROS is a pro-apoptosis factor.[37,38] Emerging evidence indicates that the upregulation of ROS is required for the initiation of apoptotic responses induced by several anti-cancer agents.[39] To further determine the potential role of oxidative stress in HTPM-induced toxicity in MDA-MB-231 cells, we examined the regulatory effects of HTPM on ROS levels using the DCFH-DA-based assay. The results showed that HTPM significantly increased ROS levels in a dose-dependent manner, which was effectively scavenged by NAC, a widely used ROS scavenger (Figure 6A). To confirm that HTPM increased apoptosis by regulating the ROS levels, we pre-treated the cells with NAC, which clearly abolished the cell apoptosis induced by HTPM. The same results were also observed in MCF-7 cells (Supplementary Materials, Figure S4A). These data suggest that HTPM induced apoptosis by regulating the levels of ROS in MDA-MB-231 and MCF-7 cells. Next, we analyzed the effects of HTPM on cell cycle progression by fluorescence-activated cell sorting. The results showed that HTPM induced marked G2-M arrest in both MDA-MB-231 and MCF-7 cells (Figure 5C and

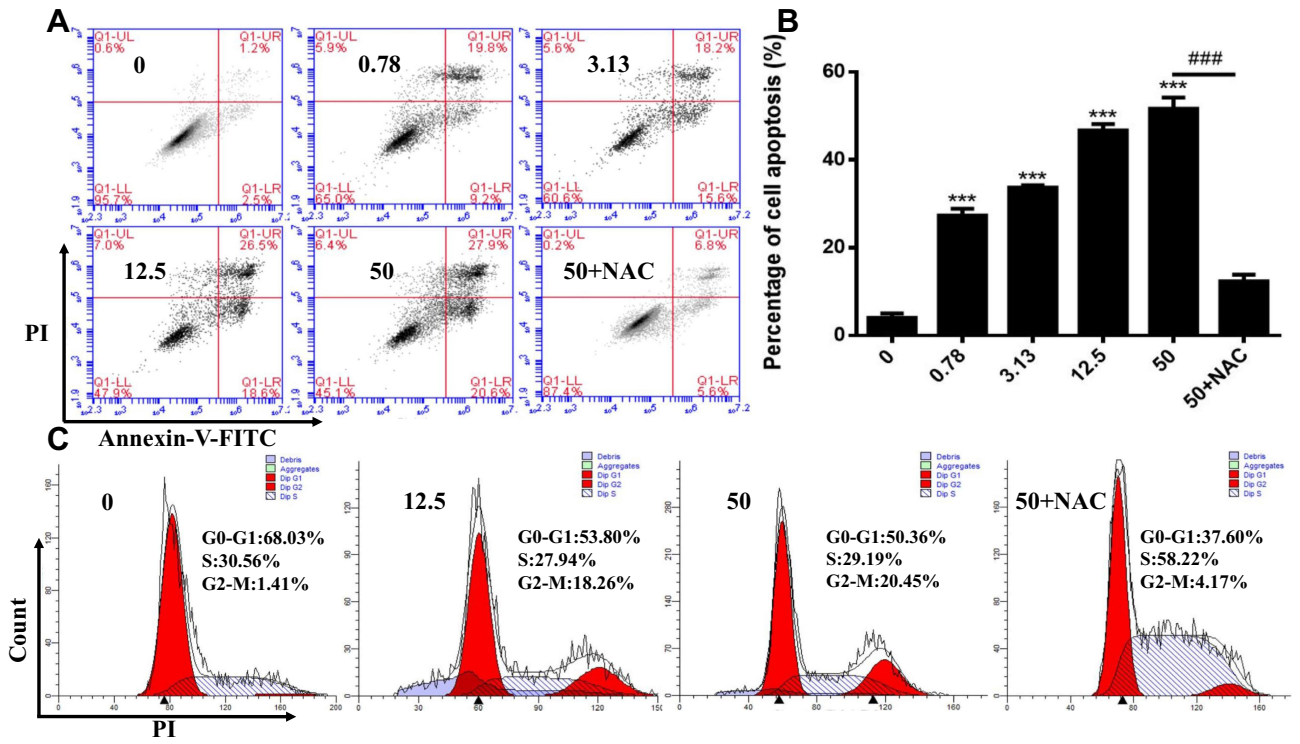

Figure 5 Effect of HTPM on apoptosis and cell cycle arrest of MDA-MB-231 cells. (**A** and **B**) The representative images and summaries of apoptosis induced by HTPM exposure in the presence or absence of NAC were presented. (**C**) The representative images and summaries of cell cycle distribution induced by HTPM exposure in the presence or absence of NAC were shown. $^{###}P<0.001$, $^{***}P<0.001$.

Supplementary Materials, Figure S3C), and these effects were abolished by NAC pre-treatment. These results collectively indicate that HTPM induces breast cancer cell apoptosis and cell cycle arrest by regulating ROS level in vitro. A sensitive effector mechanism widely engaged in the control and modulation of apoptosis is cellular redox status, which is determined by the balance between the rates of generation and breakdown of ROS.[40] ROS is a major regulator involved in apoptosis mediated through mitochondria. High levels of ROS in the mitochondria can induce several irreversible steps.[41] In addition, we confirmed that HTPM induced apoptosis by causing the accumulation of ROS. ROS inducers as anti-cancer drugs have received considerable attention due to their selective effects on cancer cells while sparing normal cells.[42]

Alteration of MMP by HTPM

Emerging evidence suggests that ROS induces apoptotic death in cancer cells by causing mitochondrial membrane damage, resulting in MMP disorder.[43,44] The change in MMP is also one sign of apoptosis. HF induces apoptosis in breast cancer cells through the mitochondria-dependent pathway.[44] The mitochondrial function depends on stabilization of the mitochondrial membrane structure.[45] The change in MMP was evaluated using a fluorescent cationic dye (JC-1), followed by flow cytometry. In healthy cells, JC-1 emitted red fluorescence at a wavelength of 590 nm. By contrast, in apoptotic cells, JC-1 exhibited green fluorescence at 525 nm. Our results indicated that HTPM disrupted the MMP (Figure 6B and C), and induced the highest level of mitochondrial depolarization in MDA-MB-231 cells after 24 h (27.8%), followed by 16.9% and 13.4% at 24 h. At the same time, HTPM induced the highest level of mitochondrial depolarization in MCF-7 cells after 24 h (28.1%), followed by 21.1% and 13.4% at 24 h (Supplementary Materials, Figure S4B, C). A decrease in MMP is often a sign of early apoptosis.[24] A previous investigation showed that HF exhibited activation effects on the mitochondrial pathway of apoptosis.[40] Our results revealed the significant reduction of MMP of MDA-MB-231 and MCF-7 cells treated with HTPM. These data suggest that HTPM may induce cell apoptosis by enhancing ROS through the mitochondrial pathway.

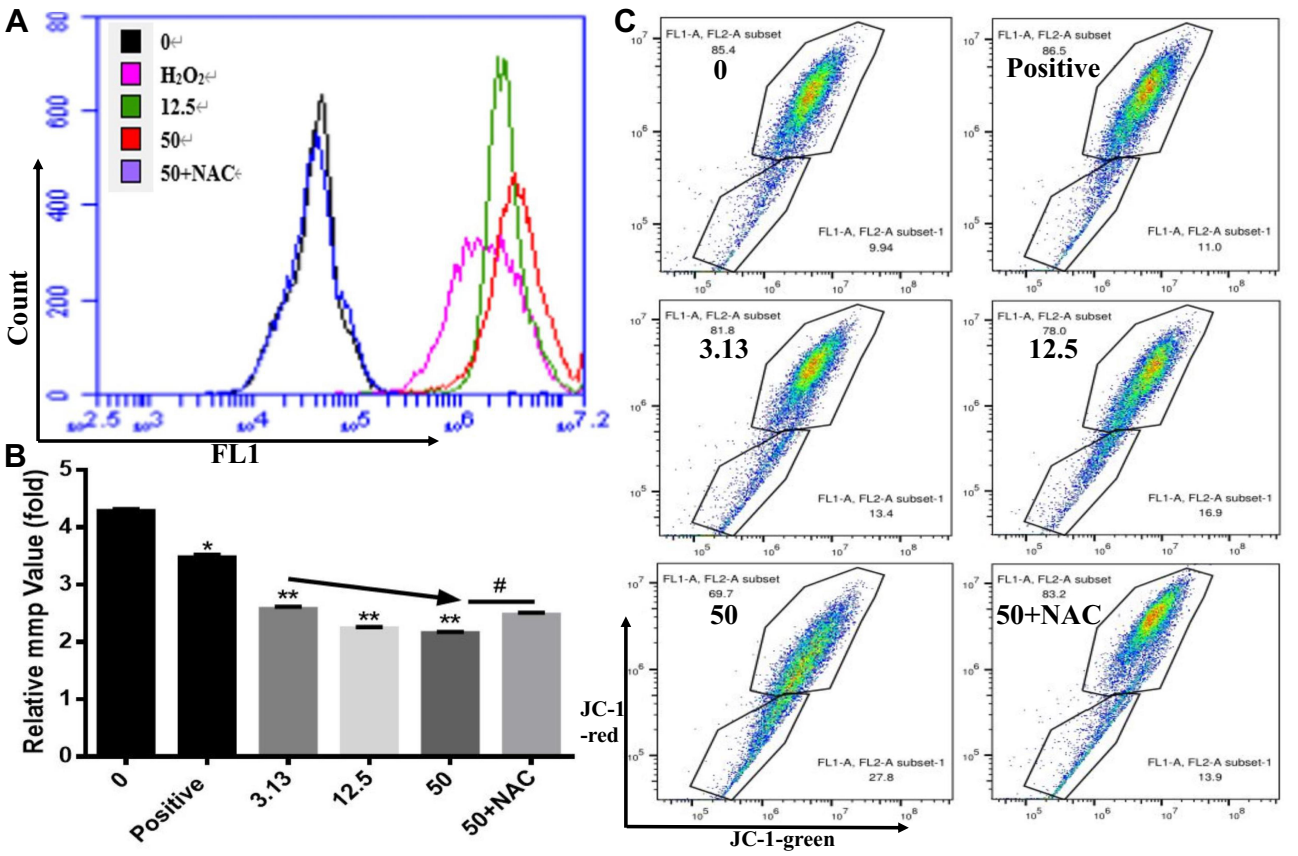

Figure 6 Influence of HTPM on reactive oxygen species (ROS) and mitochondrial membrane potential (MMP) of MDA-MB-231 cells. (**A**) The representative images of ROS generation in MDA-MB-231 cells exposed to HTPM at various concentrations in the presence or absence of antioxidants NAC. H_2O_2 was used as the positive control. (**B** and **C**) The summary and representative images of MMP alteration in MDA-MB-231 cells exposed to HTPM at various concentrations in the presence or absence of antioxidants NAC. **P*<0.05, #*P*<0.05, ***P*<0.01.

In vivo Antitumor Efficacy in Subcutaneous Tumor-Bearing Mice Model

The subcutaneous breast cancer-bearing BALB/c nude mouse model was successfully established by injecting MDA-MB-231 cells (1×10^6 cells/mouse), and was used to evaluate the in vivo anti-cancer efficacy of HTPM and free HF. As shown in Figure 7A, both HF- and HTPM-treated groups effectively inhibited tumor growth compared with the control group. Furthermore, the TIR value of HTPM treatment was 68.17 ± 1.28%, whereas that of HF treatment was only 36.82 ± 2.35%, suggesting that the HTPM group significantly outperformed the HF group in tumor inhibition. It has been reported that the volume of the tumor in the control group increased significantly with the prolongation of time, indicating that TPGS had almost no effect on inhibiting the tumor growth.[46] After stopping drug administration, tumor volumes of both treatment groups were largely increased, but the growth rate was significantly lower than that of the control group (Figure 7B). The mice were euthanized and dissected to collect the tumor samples on day 14, and photographs were taken (Figure 7C). The tumor weights in the HTPM-treated group were much lower than those in the groups treated with PBS or HF (Figure 7D). It is noteworthy that a significant increase in tumor weight occurred in the PBS- and free HF-treated groups from days 11 to 14 (Figure 7E), but only a slight weight increase was found in the HTPM-treated group, in accordance with the results in Figure 7D. These data suggested that HTPM had stronger growth inhibitory effects against breast cancer than free HF treatment groups, and showed ongoing inhibitory effects after drug withdrawal. As reported in a previous study, after IV bolus delivery to mice, HF was distributed rapidly to all tissues, except the brain. An IV dose of 1.5 mg/kg produced peak plasma HF concentrations of 313–386 ng/mL at 5 min after injection. HF persisted in lung, liver, kidney, spleen, and skeletal muscle longer than in plasma.[33] The short residence time in blood circulation and non-specific distribution in the body greatly hinder the clinical applications of anti-tumor

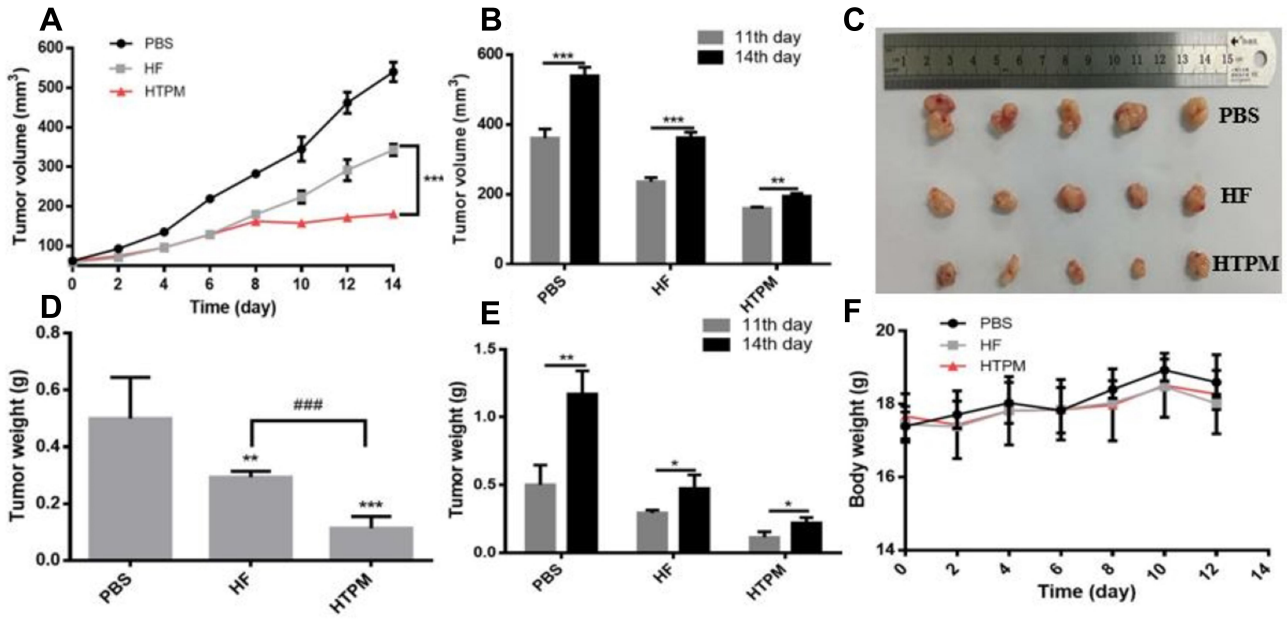

Figure 7 In vivo anti-cancer effect of intravenously injected free HF and HTPM from 0th day to 14th day in female BALB/c mice. Tumor volumes (**A** and **B**), morphology of the harvested tumors (**C**), tumor weights (**D** and **E**) and body weights (**F**) of nude mice after administration of free HF, HTPM or control (PBS) were exhibited. **P*<0.05, ***P*<0.01, ****P*<0.001, ###*P*<0.001.

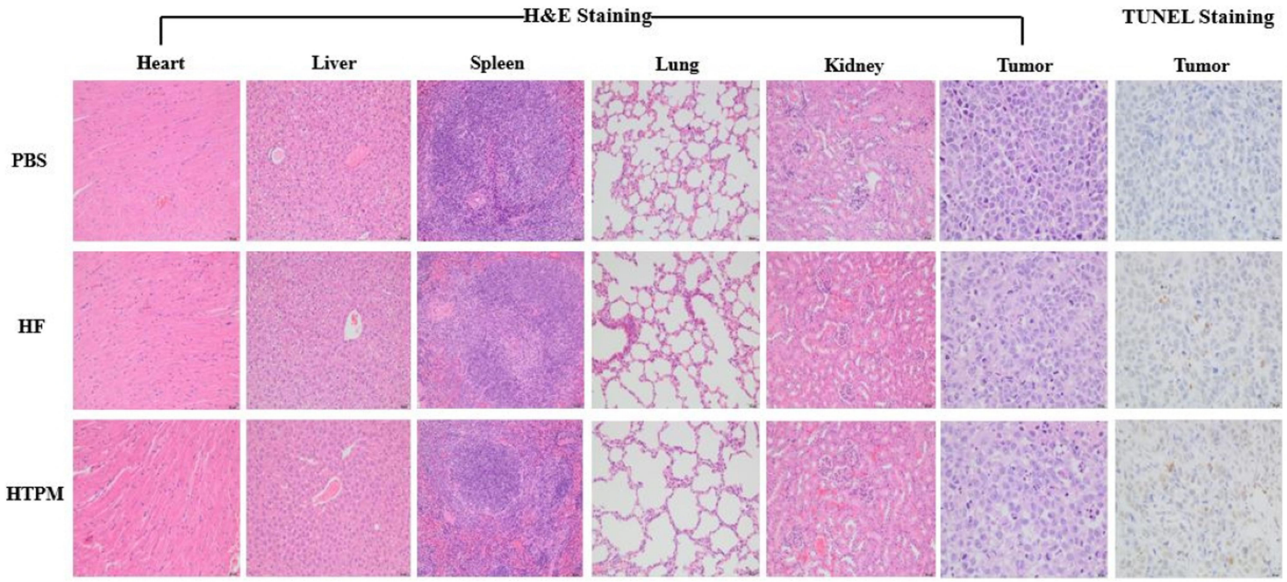

Figure 8 Histological analysis of main organs and tumors from nude mice treated with PBS, HF and HTPM using H&E staining and TUNEL staining. Images were taken at 400× magnification.

drugs.[47] TPGS PMs can extend the circulation time and half-life of drugs. For example, scutellarin has a short residence time in the circulation, which is rapidly eliminated from the blood in rabbits and dogs after a single IV dose. Scutellarin-loaded TPGS PMs exhibit a mean residence time of 1474.76 ± 35.79 min, which is 22.7-fold higher than that of commercial injection.[48] TPGS PMs can significantly prolong its half-life, leading to enhanced circulation. Most importantly, the PMs prolong the cycle time and keep the drug stable in the body. Thus, TPGS can improve the anti-tumor effects of HF, although this needs to be confirmed in follow-up studies.

Next, immunohistochemical analysis was carried out to further elucidate the anti-cancer efficacy of HTMP. H&E staining of tumor sections indicated that tumor samples from

the treated groups had a greater necrotic area compared to the control group. Tumors from the HTPM-treated group showed maximum necrosis. Furthermore, TUNEL staining of tumor tissues clearly showed significant apoptosis induced by HTPM compared with other treatments (Figure 8). Meanwhile, the chronic toxicity of these treatments was also monitored by the change in body weights and histologic analysis of major organs. The weight of mice in all groups steadily increased until the end of the experiment (Figure 7F). No distinct histologic changes were observed in the heart, liver, spleen, lung, and kidney after any treatment, suggesting that the mice tolerated all treatments well (Figure 8). These results demonstrate that TPGS can serve as an effective delivery carrier to boost the anti-cancer activity of HF against breast cancer with excellent biocompatibility.

Conclusion

In this study, HTPMs were successfully fabricated using the thin-film ultrasonic method. The optimized HTPM not only had a small size with narrow distribution, excellent stability, and sustained release behavior but also exhibited stronger inhibition than free HF and PTX against TNBCs. Furthermore, HTPM induced the apoptosis of breast cancer cells by disrupting mitochondria and enhancing ROS formation. Moreover, HTPM markedly suppressed in vivo tumor growth in tumor-bearing mice and exhibited good biocompatibility. These findings indicate that HTPM holds great therapeutic promise for TNBCs.

Highlights

- Halofuginone hydrobromide-TPGS-polymer micelles (HTPMs) were successfully fabricated using the thin-film hydration technique.
- HTPM had a small size with narrow distribution, excellent stability and sustained release behavior.
- HTPM exhibited stronger inhibition against triple-negative breast cancer cells than free halofuginone hydrobromide and paclitaxel.
- HTPM can induce apoptosis of breast cancer cells by disrupting mitochondria and enhancing reactive oxygen species formation.
- HTPM markedly suppressed the in vivo tumor growth in tumor-bearing mice and exhibited good biocompatibility.

Acknowledgments

The authors would like to acknowledge the assistance of Fang Chen from Laboratory Animal Center of Nanjing Agricultural University. This work was supported by the grants from the Fundamental Research Funds for the Central Universities (Nos. KYGD202002, WK9110000013, WK9110000120), the National Key Research and Development Program (No. 2016YFD0501306), the National Natural Science Foundation of China (No. 31672612) and a project funded by the Priority Academic Program Development of Jiangsu Higher Education Institutions.

Disclosure

The authors have no conflicts of interest to declare for this work.

References

1. Nassar A, Abouelhoda M, Mansour O, Loutfy SA, Hafez MM, Gomaa M. Targeted next generation sequencing identifies somatic mutations in a cohort of Egyptian breast cancer patients. *J Adv Res*. 2020;24:149–157. doi:10.1016/j.jare.2020.04.001
2. Zheng S, Bai JQ, Li J, et al. The pathologic characteristics of breast cancer in China and its shift during 1999–2008: a national-wide multicenter cross-sectional image over 10 years. *Int J Cancer*. 2012;131(11):2622–2631. doi:10.1002/ijc.27513
3. Kutty RV, Feng SS. Cetuximab conjugated vitamin E TPGS micelles for targeted delivery of docetaxel for treatment of triple negative breast cancers. *Biomaterials*. 2013;34(38):10160–10171. doi:10.1016/j.biomaterials.2013.09.043
4. Zhao Y, Alakhova DY, Zhao X, Band V, Batrakova EV, Kabanov AV. Eradication of cancer stem cells in triple negative breast cancer using doxorubicin/pluronic polymeric micelles. *Nanomedicine*. 2020;24:102–124.
5. Kumar MA, Bharti S, Singh P, et al. Trastuzumab decorated TPGS-g-chitosan nanoparticles for targeted breast cancer therapy. *Colloids Surf B*. 2019;173:366–377. doi:10.1016/j.colsurfb.2018.10.007
6. Diana A, Franzese E, Centonze S, et al. Triple-negative breast cancers: systematic review of the literature on molecular and clinical features with a focus on treatment with innovative drugs. *Curr Oncol Rep*. 2018;20(10):76. doi:10.1007/s11912-018-0726-6
7. Torre LA, Bray F, Siegel RL, Ferlay J, Tieulent LJ, Jemal A. Global cancer statistics 2012. *CA Cancer J Clin*. 2015;65(2):87–108. doi:10.3322/caac.21262
8. Guzmán-Rodríguez JJ, Ochoa-Zarzosa A, López-Gómez R, López-Meza JE. Plant antimicrobial peptides as potential anticancer agents. *Biomed Res Int*. 2015;2015:735087.
9. Di LA, Gomez HL, Aziz Z, et al. Phase III, double-blind, randomized study comparing lapatinib plus paclitaxel with placebo plus paclitaxel as first-line treatment for metastatic breast cancer. *J Clin Oncol*. 2008;26(34):5544–5552. doi:10.1200/JCO.2008.16.2578
10. Abu Samaan TM, Samec M, Liskova A, Kubatka P, Büsselberg D. Paclitaxel's mechanistic and clinical effects on breast cancer. *Biomolecules*. 2019;9(12):789. doi:10.3390/biom9120789
11. Wang H, Zhao Y, Wu Y, et al. Enhanced anti-tumor efficacy by co-delivery of doxorubicin and paclitaxel with amphiphilic methoxy PEG-PLGA copolymer nanoparticles. *Biomaterials*. 2011;32(32):8281–8290. doi:10.1016/j.biomaterials.2011.07.032
12. Zhang DF, Sun BB, Yue YY, et al. Anticoccidial effect of halofuginone hydrobromide against *Eimeria tenella* with associated histology. *Parasitol Res*. 2012;111(2):695–701. doi:10.1007/s00436-012-2889-7
13. Xia X, Wang L, Zhang X, et al. Halofuginone-induced autophagy suppresses the migration and invasion of MCF-7 cells via regulation of STMN1 and p53. *J Cell Biochem*. 2018;119(5):4009–4020. doi:10.1002/jcb.26559

14. Chen GQ, Gong RH, Yang DJ, et al. Halofuginone dually regulates autophagic flux through nutrient-sensing pathways in colorectal cancer. *Cell Death Dis*. 2017;8(5):e2789. doi:10.1038/cddis.2017.203
15. Wang Y, Xie Z, Lu H. Significance of halofuginone in esophageal squamous carcinoma cell apoptosis through HIF-1α-FOXO3a pathway. *Life Sci*. 2020;257:118104. doi:10.1016/j.lfs.2020.118104
16. Nagler A, Ohana M, Shibolet O, et al. Suppression of hepatocellular carcinoma growth in mice by the alkaloid coccidiostat halofuginone. *Eur J Cancer*. 2004;40(9):1397–1403. doi:10.1016/j.ejca.2003.11.036
17. De Figueiredo-pontes LL, Assis PA, Santana-Lemos BA, et al. Halofuginone has anti-proliferative effects in acute promyelocytic leukemia by modulating the transforming growth factor beta signaling pathway. *PLoS One*. 2011;6(10):e26713. doi:10.1371/journal.pone.0026713
18. Koohestani F, Qiang W, MacNeill AL, et al. Halofuginone suppresses growth of human uterine leiomyoma cells in a mouse xenograft model. *Hum Reprod*. 2016;31(7):1540–1551. doi:10.1093/humrep/dew094
19. Li X, Wang Y, Sun N, et al. Biopharmaceutical classification system research for six commonly used anti-parasitic drugs in chickens. *J Nanjing Agric Univ*. 2020;43(5):919–926.
20. Li W, Xue J, Xu H. Combined administration of PTX and S-HM-3 in TPGS/Solutol micelle system for oncotarget therapy. *Int J Nanomedicine*. 2019;14:1011–1026. doi:10.2147/IJN.S189864
21. Fang Z, Pan S, Gao P, et al. Stimuli-responsive charge-reversal nano drug delivery system: the promising targeted carriers for tumor therapy. *Int J Pharm*. 2020;575:118841. doi:10.1016/j.ijpharm.2019.118841
22. Guo Y, Luo J, Tan S, Otieno BO, Zhang Z. The applications of vitamin E TPGS in drug delivery. *Eur J Pharm Sci*. 2013;49(2):175–186. doi:10.1016/j.ejps.2013.02.006
23. Yang C, Wu T, Qi Y, Zhang Z. Recent advances in the application of vitamin E TPGS for drug delivery. *Theranostics*. 2018;8(2):464–485. doi:10.7150/thno.22711
24. Choudhury H, Gorain B, Pandey M, et al. Recent advances in TPGS-based nanoparticles of docetaxel for improved chemotherapy. *Int J Pharm*. 2017;529(1–2):506–522. doi:10.1016/j.ijpharm.2017.07.018
25. Jin ML, Park SY, Kim YH, Park G, Lee SJ. Halofuginone induces the apoptosis of breast cancer cells and inhibits migration via down-regulation of matrix metalloproteinase-9. *Int J Oncol*. 2014;44(1):309–318. doi:10.3892/ijo.2013.2157
26. Leiba M, Jakubikova J, Klippel S, et al. Halofuginone inhibits multiple myeloma growth in vitro and in vivo and enhances cytotoxicity of conventional and novel agents. *Br J Haematol*. 2012;157(6):718–731. doi:10.1111/j.1365-2141.2012.09120.x
27. Augustine R, Kim DK, Kalva N, Eom KH, Kim JH, Kim I. Multi-stimuli-responsive nanomicelles fabricated using synthetic polymer polylysine conjugates for tumor microenvironment dependent drug delivery. *J Mater Chem B*. 2020;8(26):5745–5755. doi:10.1039/D0TB00721H
28. Blanco E, Kessinger CW, Sumer BD, Gao J. Multifunctional micellar nanomedicine for cancer therapy. *Exp Biol Med (Maywood)*. 2009;234(2):123–131. doi:10.3181/0808-MR-250
29. Wang R, Yang M, Li G, et al. Paclitaxel-betulinic acid hybrid nanosuspensions for enhanced anti-breast cancer activity. *Colloids Surf B*. 2019;174:270–279. doi:10.1016/j.colsurfb.2018.11.029
30. Sun L, Wei H, Zhang X, et al. Synthesis of polymeric micelles with dual-functional sheddable PEG stealth for enhanced tumor-targeted drug delivery. *Polym Chem*. 2020;11(27):4469–4476. doi:10.1039/D0PY00653J
31. Deng X, Lin D, Zhang X, et al. Profiles of immune-related genes and immune cell infiltration in the tumor microenvironment of diffuse lower-grade gliomas. *J Cell Physiol*. 2020;235(10):7321–7331. doi:10.1002/jcp.29633
32. Hammad RW, Sanad RA, Abdelmalak NS, Torad FA, Latif R. New intranasal cross-linked mosapride xyloglucan pluronics micelles (MOS-XPMs) for reflux esophagitis disease: in-vitro optimization and improved therapeutic efficacy. *J Adv Res*. 2020;23:83–94. doi:10.1016/j.jare.2020.01.013
33. Stecklair KP, Hamburger DR, Egorin MJ, Parise RA, Covey JM, Eiseman JL. Pharmacokinetics and tissue distribution of halofuginone (NSC 713205) in CD2F1 mice and Fischer 344 rats. *Cancer Chemother Pharmacol*. 2001;48(5):375–382. doi:10.1007/s002800100367
34. Hao T, Chen D, Liu K, et al. Micelles of d-α-tocopheryl polyethylene glycol 2000 succinate (TPGS 2K) for doxorubicin delivery with reversal of multidrug resistance. *ACS Appl Mater Interfaces*. 2015;7(32):18064–18075. doi:10.1021/acsami.5b04995
35. Yan W, Yang J, Tang H, et al. Flavonoids from the stems of Millettia pachyloba Drake mediate cytotoxic activity through apoptosis and autophagy in cancer cells. *J Adv Res*. 2019;20:117–127. doi:10.1016/j.jare.2019.06.002
36. P K A, Binder MJ, Walder K, Puri M. Recombinant balsamin induces apoptosis in liver and breast cancer cells via cell cycle arrest and regulation of apoptotic pathways. *Process Biochem*. 2020;96:146–156. doi:10.1016/j.procbio.2020.05.029
37. Fang XL, Cao JJ, Shen AZ. Advances in anti-breast cancer drugs and the application of nano-drug delivery systems in breast cancer therapy. *J Drug Deliv Sci and Tec*. 2020;57:e101662. doi:10.1016/j.jddst.2020.101662
38. Sun ZP, Zhang J, Shi LH, et al. Aminopeptidase N inhibitor 4cc synergizes antitumor effects of 5-fluorouracil on human liver cancer cells through ROS-dependent CD13 inhibition. *Biomed Pharmacother*. 2015;76:65–72. doi:10.1016/j.biopha.2015.10.023
39. Na HK, Kim EH, Choi MA, Park JM, Kim DH, Surh YJ. Diallyl trisulfide induces apoptosis in human breast cancer cells through ROS-mediated activation of JNK and AP-1. *Biochem Pharmacol*. 2012;84(10):1241–1250. doi:10.1016/j.bcp.2012.08.024
40. Zhang Y, Luo M, Zu Y, et al. Dryofragin, a phloroglucinol derivative, induces apoptosis in human breast cancer MCF-7 cells through ROS-mediated mitochondrial pathway. *Chem Biol Interact*. 2012;199(2):129–136. doi:10.1016/j.cbi.2012.06.007
41. Huang P, Feng L, Oldham EA, Keating MJ, Plunkett W. Superoxide dismutase as a target for the selective killing of cancer cells. *Nature*. 2000;407(6802):390–395. doi:10.1038/35030140
42. Petanidis S, Kioseoglou E, Hadzopoulou-Cladaras M, Salifoglou A. Novel ternary vanadium-betaine-peroxido species suppresses H-ras and matrix metalloproteinase-2 expression by increasing reactive oxygen species-mediated apoptosis in cancer cells. *Cancer Lett*. 2013;335(2):387–396. doi:10.1016/j.canlet.2013.02.052
43. Yang LL, Wang PS, Wang HX, et al. Fucoidan derived from *Undaria pinnatifida* induces apoptosis in human hepatocellular carcinoma SMMC-7721 cells via the ROS-mediated mitochondrial pathway. *Mar Drugs*. 2013;11(6):1961–1976. doi:10.3390/md11061961
44. Yang F, Chen WD, Deng R, et al. Hirsutanol A, a novel sesquiterpene compound from fungus Chondrostereum sp., induces apoptosis and inhibits tumor growth through mitochondrial-independent ROS production: hirsutanol A inhibits tumor growth through ROS production. *J Transl Med*. 2013;11(6):1961–1976. doi:10.1186/1479-5876-11-32
45. Green DR, Kroemer G. The pathophysiology of mitochondrial cell death. *Science*. 2004;305(5684):626–629. doi:10.1126/science.1099320
46. Xu Y, Meng H, Du F, et al. Preparation of intravenous injection nanoformulation of VESylated gemcitabine by co-assembly with TPGS and its anti-tumor activity in pancreatic tumor-bearing mice. *Int J Pharm*. 2015;495(2):792–797. doi:10.1016/j.ijpharm.2015.09.030
47. Zhao D, Zhang H, Tao W, Wei W, Sun J, He Z. A rapid albumin-binding 5-fluorouracil prodrug with a prolonged circulation time and enhanced antitumor activity. *Biomater Sci*. 2017;5(3):502–510. doi:10.1039/C6BM00884D
48. Zou L, Xiong SJ, Deng XP, Liu J, Xiong RD, Wang Z. Preparation of scutellarin loaded TPGS polymeric micelles and evaluation of its pharmacokinetics and pharmacodynamics effects in rats. *Acta Pol Pharm*. 2018;75(6):1305–1312.